LANGMUIR Article
Cite This: Langmuir 2019, 35, 9050−9060
pubs.acs.org/Langmuir

Surfactant Charge Modulates Structure and Stability of Lipase-Embedded Monolayers at Marine-Relevant Aerosol Surfaces

Man Luo,[†,∥] Abigail C. Dommer,[†,∥] Jamie M. Schiffer,[‡] Donald J. Rez,[†] Andrew R. Mitchell,[†] Rommie E. Amaro,*[,†] and Vicki H. Grassian*[,†,§]

[†]Department of Chemistry and Biochemistry, University of California, San Diego, California 92093, United States
[‡]Janssen Pharmaceuticals, 3210 Merryfield Row, San Diego, California 92093, United States
[§]Scripps Institution of Oceanography, University of California, San Diego, California 92037, United States

Supporting Information

ABSTRACT: Lipases, as well as other enzymes, are present and active within the sea surface microlayer (SSML). Upon bubble bursting, lipases partition into sea spray aerosol (SSA) along with surface-active molecules such as lipids. Lipases are likely to be embedded in the lipid monolayer at the SSA surface and thus have the potential to influence SSA interfacial structure and chemistry. Elucidating the structure of the lipid monolayer at SSA interfaces and how this structure is altered upon interaction with a protein system like lipase is of interest, given the importance of how aerosols interact with sunlight, influence cloud formation, and provide surfaces for chemical reactions. Herein, we report an integrated experimental and computational study of *Burkholderia cepacia* lipase (BCL) embedded in a lipid monolayer and highlight the important role of electrostatic, rather than hydrophobic, interactions as a driver for monolayer stability. Specifically, we combine Langmuir film experiments and molecular dynamics (MD) simulations to examine the detailed interactions between the zwitterionic dipalmitoylphosphatidylcholine (DPPC) monolayer and BCL. Upon insertion of BCL from the underlying subphase into the lipid monolayer, it is shown that BCL permeates and largely disorders the monolayer while strongly interacting with zwitterionic DPPC molecules, as experimentally observed by Langmuir adsorption curves and infrared reflectance absorbance spectroscopy. Explicitly solvated, all-atom MD is then used to provide insights into inter- and intramolecular interactions that drive these observations, with specific attention to the formation of salt bridges or ionic-bonding interactions. We show that after insertion into the DPPC monolayer, lipase is maintained at high surface pressures and in large BCL concentrations by forming a salt-bridge-stabilized lipase−DPPC complex. In comparison, when embedded in an anionic monolayer at low surface pressures, BCL preferentially forms intramolecular salt bridges, reducing its total favorable interactions with the surfactant and partitioning out of the monolayer shortly after injection. Overall, this study shows that the structure and dynamics of lipase-embedded SSA surfaces vary based on surface charge and pressure and that these variations have the potential to differentially modulate the properties of marine aerosols.

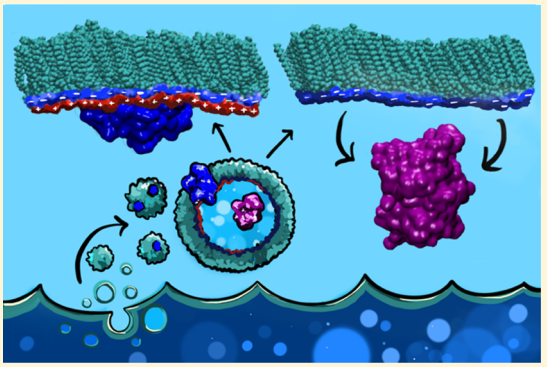

INTRODUCTION

The lipid monolayer interface has largely been studied for its biological relevance—monolayers occur in the body as lung surfactants and tear films—but is also of great interest to the atmospheric chemistry community for its role in modulating sea spray aerosol (SSA) particle reactions and dynamics.[1−9] Lipid monolayers are known to coat the ocean surface and the surface of nascent SSA and can significantly impact SSA climate-relevant properties.[3−5,7−11] It has been shown that the lipid type and composition of SSA surfaces have all been found to influence hygroscopicity,[3,6] cloud condensation nucleation activity,[3,5,6] and ice nucleation activity of SSA.[4,11] Amphiphilic lipids can impact interfacial properties of SSA primarily because they are surface-active. Surfactants such as phospholipids participate in photooxidation and ozonolysis,[12] their anionic headgroups selectively bind and concentrate trace metal cations at the surface,[13−15] and their carbon chain length and headgroup charge(s) influence the transport and reactivity of gases at the interface.[7−9] While the chemical composition of SSA and their effects on climate are becoming more resolved, the molecular structure and dynamics of SSA surfaces remain difficult to probe experimentally.[16−23] Computational methods such as all-atom molecular dynamics (MD) have therefore contributed largely to the existing body of work on the lipid monolayer interface.[24−27] Since computational methods can resolve chemical systems at the atomic level, the integration of computation with experimental aerosol techniques is expected to significantly advance our ability to model the SSA

Received: March 7, 2019
Revised: May 13, 2019
Published: June 12, 2019

DOI: 10.1021/acs.langmuir.9b00689
Langmuir 2019, 35, 9050−9060

interface.[28] The present study thus takes an integrated computational and experimental approach to understand how the lipid monolayer surface of SSA is affected by the presence of lipase.

Of particular importance to this work, lipases, as well as other enzymes, have been previously found in nascent SSA and remain active after aerosolization with consequences for aerosol reactivity.[19] Lipases catalyze the breakdown of high-order glycerides into their respective fatty acids.[29−31] *Burkholderia cepacia* lipase (BCL), the lipase used in this study, is produced by a complex of bacterial species commonly found in marine environments.[32,33] In SSA, free lipases can either have been secreted by marine bacteria or released as their bacterial cells lyse during aerosolization.[34,35] A recent study on BCL embedded in diphenylphosphoryl azide (DPPA), palmitic acid, and palmitate bilayers shows that the BCL structure is highly dependent on its immediate chemical environment, suggesting that subtle variations in SSA lipid composition and surface pressure could have drastic effects on its activity.[36−38] Although it is currently unknown whether lipases embedded in lipid monolayers, rather than bilayers, retain their activity, BCL, in particular, is known to be structurally and functionally robust; it is able to retain its conformation and catalytic activity in various aqueous environments, across a broad pH range, and in the presence of high organic solvent concentrations.[39−41] In the context of SSA surface chemistry, the presence of an active lipase enzyme at the surface would mean that the surface properties of the particle are dynamic and change over time. If lipases process lipids at the surface of SSA, there would be a flux in surface pressure, charge distribution, and even overall stability and solubility of the monolayer as the particle ages.[13,25,42−45] Furthermore, bioaerosols containing a proteinaceous material provide a host of additional reactive sites that readily participate in processes such as radical photochemistry, nitration by gaseous NO_3, and ozonolysis.[46−48] The biotransformation of SSA by lipase is thus of direct relevance to atmospheric chemistry.

In addition to directly modifying the chemical composition of SSA, lipases are also likely to alter interfacial chemistry through intermolecular interactions with surrounding surfactants.[36] The lipid population at SSA surfaces is not necessarily dominated by the enzyme substrate. Rather, at the surface is a complex mixture of fatty acids, phospholipids, triglycerides, and many other organic components, meaning that folded and functional lipases will not always chemically process their surroundings.[5,11,16,20,23] For example, BCL induces lipid curvature when embedded in DPPA bilayers, a finding which is unsurprising given that membrane-embedded proteins are well known to structurally modulate their surrounding chemical environment and vice versa.[36,49−51] The lipid−lipase interactions are likely to be impacted by the lipid type and headgroup charge, as these influence hydrogen bonding, van der Waal's forces, and salt bridges. One of the goals of the present study is to characterize the dominant intermolecular interactions between lipase and both charge-balanced zwitterionic and negatively charged surfactant monolayers and to understand how these interactions might affect SSA surface chemistry.

Here, we integrate infrared reflectance absorbance spectroscopy (IRRAS) combined with Langmuir trough techniques with all-atom MD simulations to characterize the surface properties of model lipase-embedded monolayer systems. We investigate BCL interactions with two atmospherically relevant lipids, zwitterionic dipalmitoylphosphatidylcholine (DPPC) and anionic DPPA, both of which form stable monolayer films at air−aqueous interfaces. In SSA, these lipids originate in bacterial cell membranes and are released when bacterial cells lyse due to cell death or through the aerosolization process.[34,35] While nascent SSA surfaces are likely to be heterogeneous mixtures of phospholipids and fatty acids,[16] homogeneous monolayers were selected for the present study to reduce the complexity of real-world systems and allow for a careful examination of lipase−surfactant interactions. DPPA has a similar chemical structure to DPPC; both are glycerophospholipids containing two 16-carbon, saturated hydrocarbon chains, with the exception that DPPC contains a positively charged quaternary ammonium moiety attached to the negatively charged phosphate headgroup. BCL dynamics in DPPA at low surface pressure have been studied previously; DPPC was selected for this work because the effects of zwitterionic lipids on lipase are not well understood.[36] IRRAS is used to extract information about surfactant organization and ordering, coupled with a film balance and a Langmuir trough to assess the effects of varying surface pressure on BCL-embedded monolayers. All-atom MD is then used to model protein−lipid interactions, lipid interactions, and protein structure and dynamics to inform the analysis of the experimental data. Understanding the reciprocal interactions between lipid monolayers and lipase can help us better understand the structural and chemical properties of nascent SSA.

EXPERIMENTAL SECTION

Materials and Sample Preparation. Lipase from *Pseudomonas cepacia* (≥30 U/mg) was purchased from Sigma-Aldrich. Lipids (DPPA and DPPC) (>99%) were from Avanti Polar Lipids. Chloroform (>99.9%) was from Fisher Scientific. The agents above were used without further purification. The DPPC solution was prepared in chloroform with a concentration of 1 mg/mL, and the DPPA solution was prepared in a 4:1 chloroform/methanol solution with a concentration of 0.42 mg/mL.[52,53] Milli-Q water with an electric resistance of 18.2 MΩ was used for the aqueous subphase. NaCl salt purchased from Fisher Scientific was purified by baking at 200 °C overnight to remove organic contaminants and was prepared as a 0.4 M salt water solution. The concentration of the NaCl solution was chosen to be near the seawater concentration. The lipase solution was made in 0.4 M NaCl with a concentration of 4.55 mg/mL. The pH of the subphase was around 5.5, which is within the range of aerosol acidity.[45,53]

Langmuir Surface Adsorption Curve. A computer-controlled film balance with a Langmuir trough (KSV NIMA LB, S/N AAAA100505) was used for performing the surface adsorption experiments while holding the surface pressure constant. A water circulator (Beckman Geneline Cooler) controlled the temperature of the subphase in the trough at 22 °C. The lipid solution was first spread onto the 55 mL subphase in the trough using a microsyringe. The monolayer was then left for 20 min in order for the solvent to evaporate. After that, the monolayer was compressed to the desired surface pressure and held at this surface pressure. A 0.2 mL lipase solution was injected with a syringe coupled with a Teflon tubing on the needle underneath the lipid monolayer, as described previously.[36] The final concentrations of lipase in the subphase were 250, 500, 1000, or 1350 nM. The change in molecular area was monitored throughout the experiment while holding the surface pressure constant.

We performed holding area experiments using the computer-controlled film balance with a slightly modified side hole Petri dish, designed by Allen and co-workers.[15] The lipid monolayer was first

DOI: 10.1021/acs.langmuir.9b00689
Langmuir 2019, 35, 9050−9060

formed on the surface of a 55 mL subphase in the Petri dish. The lipase solution was then injected underneath the monolayer through the side hole after 30 min, and the final concentration of lipase in the subphase was 500 nM. While the area was kept constant, the surface pressure was monitored with the computer-controlled film balance throughout the experiment.

Infrared Reflection Absorption Spectroscopy (IRRAS) System. The IRRAS setup has been described previously.[12] The IR beam from an infrared spectrometer (Bruker Tensor 37) is directed onto the aqueous solution surface in the Langmuir trough or the side hole Petri dish at a 30° angle from the surface. At an air−water interface, the optimal angle for the incident beam is 0−40° when an unpolarized beam is used.[54,55] The reflected beam is collected and sent to an MCT detector (Infrared Associates Inc., midband with ZnSe window). Each IRRAS spectrum is an average of 300 scans with a spectral resolution of 4 cm^{-1}. Due to the low signal and water vapor interference in other regions, here, we focus only on the C−H stretching region. For some of the experiments, the IRRAS spectrum was taken every 30 min throughout the experiment, and some were taken once at the beginning and once at the end. The reflectance absorbance (RA) for the IRRAS spectra was plotted as a function of wavenumber, where

$$\mathrm{RA} = -\log(R/R_0) \quad (1)$$

and R is the reflectivity of the film-covered surface, while R_0 is the reflectivity of the aqueous subphase.

Molecular Dynamics System Preparation. All monolayer systems were set up using CHARMM-GUI in 0.4 M NaCl at 298.15 K and were composed of a rectangular box with periodic boundary conditions.[56] Two lipid monolayer leaflets containing molecules of either DPPA or DPPC were placed above and below a TIP3P water slab, creating two interfaces in the *xy*-plane, with air (vacuum) on either side. The *xy*-dimensions of the box were 100 × 100 Å, while the total length of the box in the *z*-direction was 300 Å. A diagram of the system setup is given in Figure S1. TIP3P was selected due to its high compatibility with the CHARMM36 force field for lipids.[57] Following routine protocols for monolayer simulations, vacuum was used at the air side of the air−aqueous interfaces to approximate the density of gases in the atmosphere.[24−26,58] The lipase starting structure used for protein−lipid systems was based on the PDB entry 3LIP, with protonation states for all amino acids assigned for a pH 6 system through the Schrödinger protein preparation wizard.[59,60] For a mean molecular area (MMA) of 47 $Å^2$/lipid, 212 DPPC or DPPA molecules were placed in each leaflet. For leaflets containing lipase, the lipase was placed in the center of the leaflet at an orientation calculated using the orientation of proteins in membrane database and server and surrounded by 179 lipid molecules.[61] Each system built consisted of approximately 100 000−120 000 atoms. All systems were prepared for simulation with GROMACS and parametrized using the CHARMM36 force field.[57,62,63] The monolayers were energy-minimized and equilibrated in six equilibration steps using GROMACS 2018 on an NVIDIA GTX 1080Ti GPU (GeForce GTX Titan, NVIDIA, Santa Clara, CA). The energy minimization and equilibration steps are described in the Supporting Information.

Molecular Dynamics Simulations and Data Analysis. Production steps for each system were run for approximately 400 ns total with three replicates under an NVT ensemble, an ensemble commonly used for monolayer simulations.[25,26,58] For lipase in each DPPA and DPPC, replicates 1, 2, and 3 were run for 100, 100, and 200 ns, respectively. The systems were assumed to be fully equilibrated when energy, root-mean-square deviation (RMSD), and solvent-accessible surface areas (SASAs) converged (Figure S2). All production runs utilized the extreme science and engineering discovery environment, which is supported by the National Science Foundation grant number ACI-1548562.[64] Specifically, simulations were performed on the Bridges supercomputer, which is supported by NSF award number ACI-1445606 at the Pittsburgh Supercomputing Center.[65] The production run script is given in full in Figure S3.

Molecular simulation data was analyzed in the IPython Jupyter Notebook environment, and all IPython notebooks for this work will be made available as part of the UCSD Library Digital Collections: Center for Aerosol Impacts on Chemistry of the Environment (CAICE) (https://library.ucsd.edu/dc/collection/bb96275693).[66]

RESULTS AND DISCUSSION

Lipase Insertion Disrupts the Lipid Monolayer as Evidenced by Experimental and Computational Methods. A Langmuir trough coupled with IRRAS spectroscopy was used to interrogate the impact of lipase on the surface properties of a DPPC monolayer. The isotherm of DPPC can be seen in Figure S4a. This isotherm has been reported in the literature..[14,67,68] We performed our holding surface pressure experiments at surface pressures of 10, 15, and 25 mN/m. In Figure 1, the Langmuir curve of the DPPC monolayer at 10 mN/m after lipase injection shows a significant increase in area (90%) within the first 5 min. Figure S5 shows that when holding the DPPC monolayer at a certain area, the surface pressure increased after lipase injection. Based on the fact that the area relaxation and pressure relaxation experiments are done with different methods, the pattern of the increasing curves between these two kinds of experiments is not comparable. Before lipase injection, the IRRAS spectra of the C−H stretching region between 2800 cm^{-1} and 3000 cm^{-1} included three peaks: the methylene symmetric stretch (2850 cm^{-1}), the methylene asymmetric stretch (2920 cm^{-1}), and the methyl asymmetric stretch (2958 cm^{-1}). From the IRRAS spectra before and 5 min after lipase injection, we observed a significant decrease in the peak intensity associated with the methylene stretch after lipase injection, as well as a broadening of the methylene stretching peaks and a shift to a higher wavenumber (Figure 1, insertion). The peak associated with the methylene asymmetric stretch shifted from 2920 to 2924 cm^{-1}. The methyl asymmetric stretch does not show a significant shift in frequency or peak broadening but instead has a small decrease in intensity. The peak at 2870 cm^{-1} after lipase injection could be associated with the methyl symmetric stretch,[54] which shows a small shoulder near the methylene symmetric stretch at 2850 cm^{-1} before lipase injection. The methyl stretch only shows a small decrease in intensity, while the methylene stretch shows a significant decrease in intensity; the peak at 2850 cm^{-1} before lipase injection disappears into

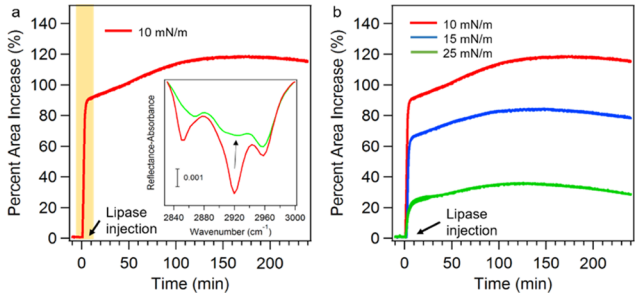

Figure 1. (a) Increase in the area of DPPC monolayer after holding at 10 mN/m induced by the injection of lipase in the underlying subphase. Inset: IRRAS spectra before (red) and 5 min after (green) lipase injection (final concentration of lipase of 500 nM). The yellow box indicates the time when the IRRAS spectra are taken. (b) Percent area increase of DPPC monolayers at 10, 15, and 25 mN/m induced by the injection of lipase into the underlying subphase (final concentration of lipase of 500 nM).

DOI: 10.1021/acs.langmuir.9b00689
Langmuir 2019, 35, 9050−9060

the methyl stretch peak at 2870 cm^{-1} upon lipase injection. The shift of the methylene groups to a higher wavenumber indicates a disordered structure of the DPPC monolayer after lipase insertion, as previous studies have found that the methylene stretching peaks shift to a higher wavenumber when entering a less ordered state.[69] Additional evidence for increased disorder for DPPC structure is seen in the peak broadening. Previous studies have found that peaks in the C−H stretching region in Raman spectra broaden when going from a more ordered crystalline state toward a more disordered state.[70−72] Conformational order information can also be obtained from the peak intensity ratio of the methylene asymmetric and methylene symmetric peaks.[70−73] This ratio changed from 1.9 to around 1.5 after lipase injection, which indicates a more disordered system induced by lipase insertion. The intensity loss can be attributed to either the increase in the mean molecular area of the DPPC molecules, indicating a lower density of DPPC molecules on the surface, or a loss of DPPC molecules through dissolution into the subphase. The IRRAS spectra collected at a longer time (greater than 5 min) remained almost the same (data not shown).

We compared the lipase−DPPC interactions at different surface pressures by injecting lipase into the DPPC monolayer and monitoring the change in the surface area increase (Figure 1b). After lipase injection, there was a fast increase followed by a slower increase in the surface area before reaching a plateau at every surface pressure studied. The total area expansion decreased with an increase in the surface pressure of DPPC, which indicates either suppression of lipase insertion or a smaller surface area of lipase embedded in the surface at higher surface pressures. This is consistent with previous experimental studies showing that, when injected into lipid monolayers, the area increase induced by lipase is reduced at higher surface pressures compared to that at lower surface pressures.[74,75] The IRRAS spectra before and after lipase injection for the DPPC monolayer at 15 and 25 mN/m are shown in Figure S6a,b, respectively. These spectra indicate that lipase has a smaller effect on DPPC structure at a higher surface pressure of 25 mN/m in comparison to that at the lower surface pressures investigated.

Molecular dynamics simulations of BCL in DPPC show that not only does lipase induce molecular disordering of DPPC but it also becomes embedded in the monolayer such that the surface of the enzyme is exposed to the atmosphere. In comparison, BCL in DPPA shows similar behavior; it fully embeds into the surfactant monolayer and disorders the surrounding lipids (Figure 2). Figure 2b gives plots of the total atmosphere-exposed surface area over the final 50 ns of each production step for lipase in DPPC and in DPPA at MMA 47 $Å^2$, a surface pressure of approximately 25 mN/m. This suggests a molecular mechanism to explain the intensity decrease and peak broadening in the IRRAS spectra. Lipase expands and embeds itself into the monolayer, decreasing the concentration of DPPC molecules at the surface and lowering the intensity of the IRRAS signal. The lipase could also contribute to the broadening of the IRRAS peaks by inducing curvature of the monolayer film. Figure 2a shows the monolayer curvature around the enzyme over the final 50 ns of simulation in DPPC and DPPA. The lipids surrounding lipase are warped, i.e., disrupted, from their hexagonal packing structure and reoriented around the lipase surface. Warping the monolayer out of the interfacial plane disrupts the C−H stretching signal, causing a decrease in and broadening of

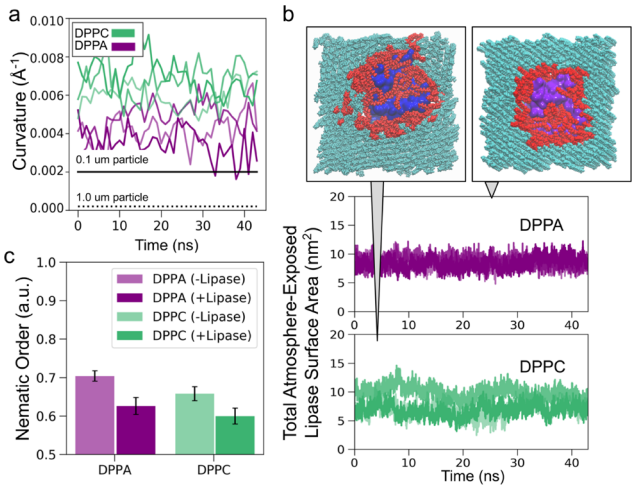

Figure 2. Data pulled from MD simulations of lipase in DPPC and comparison to DPPA at MMA 47 $Å^2$, or approximately 25 mN/m in surface pressure. (a) Quantification of monolayer curvature over the final 50 ns of each simulation replicate. Curvature was calculated using SciPy's least-squares fit; after fitting a surface to the points given by the phosphate headgroups, the inverse radius of each osculating circle in the *xz*- and *yz*-planes was extracted. The values representing the largest curvatures, in units of $Å^{-1}$, are plotted. For reference, lines corresponding to the curvatures of 0.1 and 1.0 μm particles are shown in black (solid and dotted lines, respectively). (b) Total atmosphere-exposed surface area of lipase over the final 50 ns of simulation for each replicate. Insets: Top views of lipase (blue) in DPPC (left) and lipase (purple) in DPPA (right). DPPC and DPPA molecules within 5 Å of lipase are colored red and outside of 5 Å, cyan. (c) Average nematic order parameters for lipid leaflets with and without lipase embedded. DPPA is given in purple and DPPC in green.

signal intensity.[76,77] Finally, Figure 2c shows comparisons between the nematic ordering of the lipids with and without embedded lipase. The nematic order parameter, a value between 0 and 1, is an indication of the unidirectional packing of the lipids, with 1.0 representing perfect ordering. Figure 2c shows that the nematic ordering decreases in the presence of lipase in both DPPC and DPPA. These findings are consistent with the previous studies indicating that the surrounding interfacial environment is key to lipase structure, function, and activity; however, these show this phenomenon occurring at a monolayer, rather than a bilayer or aqueous−organic interfaces.[36−38,50,51]

These results indicate that even though the lipase does not directly act upon on the surrounding lipids, it significantly alters the aerosol surface morphology with potential climate-relevant effects. For example, the insertion of lipase into SSA surfaces could increase particle hygroscopicity due to the disordering of the lipids at the interface, evidenced by the decrease in nematic order parameter and the increase in monolayer curvature. Tight-packing conformations of lipids in a monolayer film have previously been cited as a barrier to water uptake.[3,43,78,79] Early studies on mixed lipid monolayer films show a well-characterized drop in monolayer resistance in the presence of low concentrations of impurities.[80−82] At high surface pressures with highly aligned lipid-packing conformations, it can be expected that a small defect such as a disruption to the monolayer microstructure by lipase will lead to a large drop in monolayer resistance and a corresponding increase in water permeation across the interface. Because of this, it may be reasonable to suspect that lipase-containing SSA could

DOI: 10.1021/acs.langmuir.9b00689
Langmuir 2019, 35, 9050−9060

account for a portion of the cloud condensation nucleation activity of organic-enriched aerosols. Additionally, the exposure of lipase at the surface could have implications for atmospheric chemistry: proteins contain charged amino acids that easily react upon collision with atmospheric gases. For example, BCL tyrosine Y129 is exposed at the surface in our MD simulations. Tyrosine reacts readily with atmospheric ozone and NO_x species, providing one mechanism by which the biotransformation of aerosols could play a role in the atmospheric nitrogen cycle.[46]

Comparison of Lipase Interactions with Anionic DPPA and Zwitterionic DPPC Monolayers: Experimental Data. When lipase was injected under DPPC and DPPA monolayers at 25 mN/m, while lipase remained inserted in the DPPC monolayer, it crashed out of the DPPA monolayer after around 85 minutes, suggesting lower lipase stability in DPPA monolayer than in DPPC monolayer (Figure 3). The isotherm

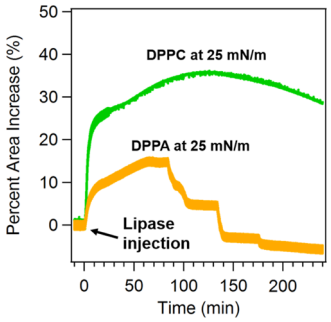

Figure 3. Percent area increase and decrease of DPPA and DPPC monolayers at 25 mN/m, induced by the injection of lipase in the underlying subphase (final lipase concentration of 500 nM).

for DPPA can be found in Figure S4b. In the previous work, BCL was reported to be stable in the DPPA monolayer at 5 mN/m, which indicates that lipase can bind with DPPA, but the protein–lipid interaction is weak compared to that of lipase with DPPC.[36] The percent area increase for DPPA before lipase crashes out is smaller than that for DPPC at the same time, which also indicates that DPPA binds weakly with lipase in comparison to DPPC. Figure 3 shows a slow decrease in the area at the end of the DPPC curve, as well as a decrease in the area below the starting point in the DPPA curve. This decrease can be partially attributed to the spontaneous dissolution of the lipids into the monolayer as previously seen for studies of long-chain fatty acid monolayers at the air–water interface.[12,83,84] Figure S7 shows that the background area decreases when the pure lipid monolayer is held at a constant 25 mN/m surface pressure. However, the area loss due to the lipid background is still less than the area loss shown in Figure 3. Therefore, this area loss can be attributed to two additional mechanisms: (i) a slight loss of lipase–lipid complex, as simulations indicate that lipids can not only be incorporated into the lipase active site but also can adhere to its surface; and (ii) the structural realignment of the lipids toward higher nematic orders (straighter hydrophobic tails), which decreases their individual molecular areas.

To test the effects of lipase concentration on its insertion into DPPC and DPPA monolayers at higher surface pressures, we performed similar experiments at 25 mN/m with different lipase concentrations. Figure 4a shows that lipase was stable in DPPC monolayers even at high lipase concentrations. The final area increase of the DPPC monolayer was dependent on the concentration of lipase used in our study (Figure 4b). In contrast, lipase was stable in DPPA monolayers only at low lipase concentrations (Figure 4c); at higher concentrations, it crashed out from the monolayer after a brief time. The "crashing-out" phenomenon is further supported by IRRAS spectra provided in Figure 4d. At high lipase concentrations (1000 nM), the area increased rapidly in the first 10 min after lipase injection, followed by a slower increase until 110 min lapsed. During this time, the IRRAS spectra (Figure 4d, left IRRAS panel) show a decrease in signal intensity and a broadening of the peaks in the C–H stretching region, indicating that lipase decreased the chain ordering of the DPPA monolayer, similar to the behavior of lipase in DPPC (Figure 1a). This disordering is confirmed by MD simulations (Figure 2c). However, after 110 min, the area gradually decreased back to its initial state, and the IRRAS spectra (Figure 4d, middle IRRAS panel) indicated an increase in signal, in which the peaks gradually recovered. For comparison, the IRRAS spectra before and after 240 min of lipase injection are presented in Figure 4d (right IRRAS panel) and appear almost the same. These IRRAS spectra indicate that almost all of the lipases inserted into the DPPA monolayer were eventually squeezed out from the interface. This "crashing-out" phenomenon has been observed previously, where Meister et al. found that the farnesylated and hexadecylated N-Ras proteins were squeezed out from the lipid monolayer at 30 mN/m, but doubly hexadecylated N-Ras proteins at the same surface pressure remained embedded.[75]

Molecular Dynamics Calculations To Further Probe and Compare Interactions between Lipase–DPPC and DPPA. To further investigate and compare the interactions between lipase and DPPA and DPPC, molecular dynamics simulations run for each system at a surface pressure of 25 mN/m were analyzed for indicators of intermolecular electrostatic interactions. To describe electrostatic interactions between the lipase and surrounding charges on the lipids, we measured instances of salt bridge formation across all trajectories. Salt bridges, defined here as ionic interactions between a positively charged nitrogen and a negatively charged oxygen, are determined to have formed if the two participating atoms enter within 3.5 Å of one another. Since salt bridge distances can be highly variable, we have selected 3.5 Å as an intermediate value within the previously reported ranges (2.8–5.0 Å) as a cutoff.[85−88] To understand the sensitivity of our distance cutoff selection, we provide error bars representing higher and lower cutoff values, 4.0 and 3.2 Å, respectively. Figure 5a shows, in color, salt bridge formation between DPPC or DPPA headgroups and lipase. We have also included in gray competing intramolecular salt bridges ("INT") that form between protein residues. This figure gives a depiction of the likelihood that specific interactions will occur.

The additional charge on zwitterionic DPPC as compared to that on anionic DPPA provides for more total interactions between the lipid headgroups and lipase (Figure S8). Both headgroups contain a negatively charged phosphate, which can interact with positively charged residues such as lysine (K, green) and arginine (R, red). However, DPPC also contains a positively charged ammonium that can interact with negatively charged surface residues such as aspartate (D, orange) and glutamate (E, purple). Figure 5a shows that not only does lipase in DPPC contain significantly more favorable electrostatic interactions than lipase in DPPA but it also contains

DOI: 10.1021/acs.langmuir.9b00689
Langmuir 2019, 35, 9050–9060

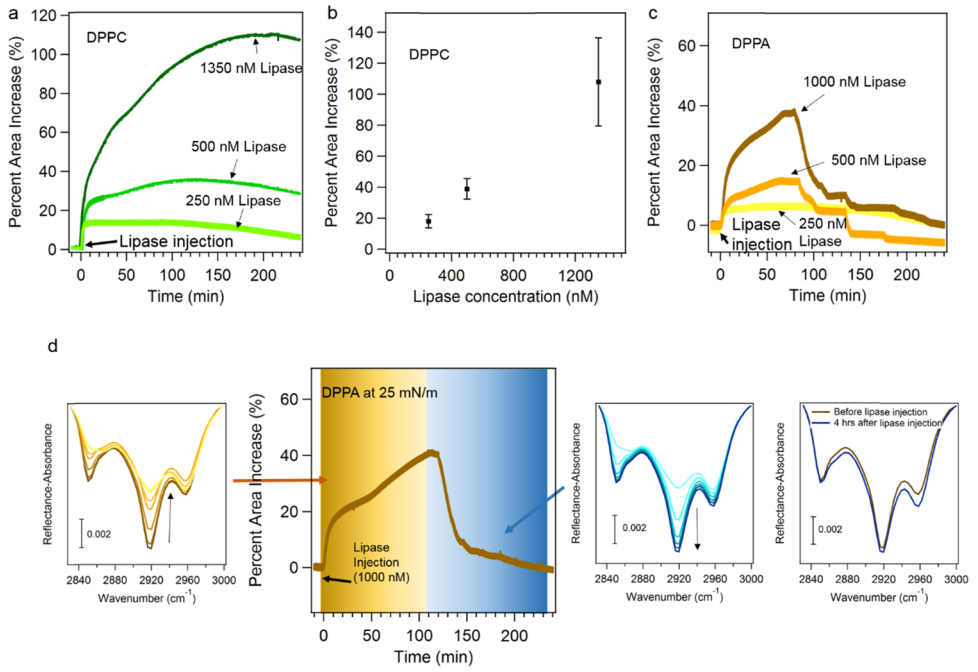

Figure 4. (a) Percent area increase of the DPPC monolayer at 25 mN/m, induced by the injection of different concentrations of lipase to the underlying subphase. (b) Percent area increase of the DPPC monolayer vs concentration of lipase in the underlying subphase. (c) Percent area increase of the DPPA monolayer at 25 mN/m induced by the injection of different concentrations of lipase into the underlying subphase. (d) Area increase and decrease of the DPPA monolayer at 25 mN/m, induced by the injection of lipase into the underlying subphase (final concentration of 1000 nM). IRRAS spectra are as follows: (left) before and 5, 10, 30, 60, 90, and 120 min after lipase injection (dark yellow to light yellow), (middle) 120, 135, 150, 180, 210, and 240 min after lipase injection (light blue to dark blue), and (right) before lipase injection (dark yellow) and 240 min after lipase injection (dark blue).

more interactions that are sustained for more than 40% of the simulation time. Additionally, DPPA coordinates strongly to sodium ions in solution (Figure S9). The negatively charged DPPA surface is stabilized by recruiting sodium cations, a process that does not occur in the neutral DPPC monolayer; thus, the charged sites on BCL compete with sodium ions for coordination with DPPA. This provides some molecular evidence to explain why lipase is more stable in DPPC than that in DPPA at high lipase concentrations, and why the percent area increase after lipase injection in DPPA is significantly smaller than in DPPC.

Figure 5b shows all intramolecular salt bridges that occur between the two lipase systems. For BCL in DPPA, the high prevalence of competing intramolecular salt bridges (Figure 5a), as well as the number and duration of total intramolecular salt bridges (Figure 5b), suggests that when BCL is surrounded by negative charges, it favors more intramolecular electrostatic interactions than BCL in DPPC. Compared to BCL embedded in DPPC, not only is there a larger percentage of available enzyme sites that have competing interactions but those interactions also appear to be stabilized for longer portions of the simulation time. This suggests that in anionic surfactants, BCL derives its structural stability from internal electrostatics, supporting experimental evidence that shows decreased BCL-embedded monolayer lifetimes and a decreased BCL-induced percent area increase for DPPA. Conversely, BCL readily complexes with zwitterionic DPPC surfactants, which allows the DPPC surface to sustain the embedded lipase at high concentrations and for longer time periods.

Our results suggest that electrostatics modulate the ability of lipase to embed in a lipid monolayer. Previous all-atom MD studies have attributed the orientation of BCL at aqueous–organic interfaces to the degree of hydrophobicity of the organic phase, which functionally stabilizes the enzyme in its open conformation as lipids are oriented into the active site.[72,73] The mechanism of BCL orientation in a lipid monolayer is similar. The hydrophobic lid helices (α9, 4, and 5) that flank the catalytic pocket (Figure S10) are immersed into the organic layer, and the remaining hydrophilic portion of the lipase is exposed to aqueous solvent (Figures 6b,d and S10). However, the phospholipid monolayers used in this work are modified aqueous–organic interfaces; the headgroups are charged, and the length of the hydrophobic tails limits the depth of the organic "phase". At low surface pressures, it is possible that lipase stability at a monolayer interface is hindered by a decreased organic phase depth and enhanced only in the presence of both positive and negative charges.

Considering our experimental and simulation data together, we provide a hypothesis to explain the rapid and discontinuous loss of area from the lipase-embedded DPPA monolayer seen in Figure 3. Due to the low intermolecular interactions between BCL and DPPA, it is possible that the lipases form small islands in the DPPA monolayer and then desorb from the monolayer together as aggregates. At low surface pressures, the hydrophobic lid residues on BCL drive the lipases to the surface. Initially, the lipases are likely to be evenly distributed throughout the monolayer. However, the insertion of the lipases causes a disruption to the lipid ordering (Figures 1a, 2c, and 4d), decreasing the van der Waal's interactions between the hydrophobic tails. Since DPPA favors higher nematic orders (Figure 2c), over time, the monolayer undergoes structural rearrangement to align the lipids back together (Figures 1a and 4d), leading to the slow decrease in area; the

DOI: 10.1021/acs.langmuir.9b00689
Langmuir 2019, 35, 9050–9060

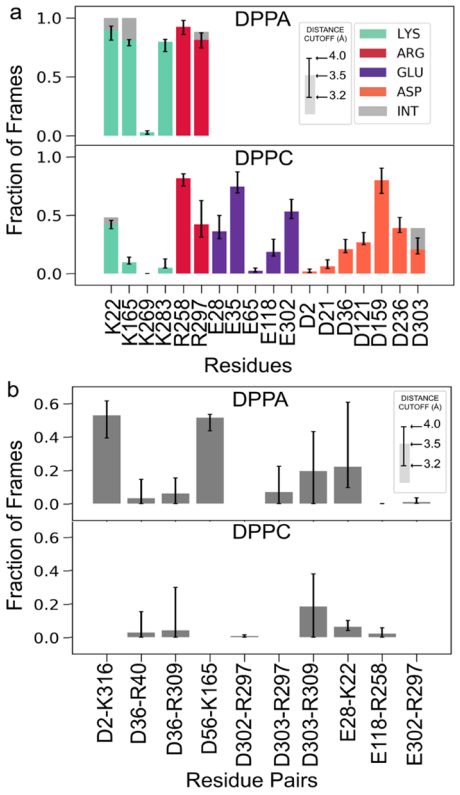

Figure 5. Lipase forms more intermolecular salt bridges with DPPC than that with DPPA but forms more intramolecular salt bridges in DPPA than in DPPC. Error bars are provided to indicate the sensitivity of the analysis to the distance cutoff selection. (a) Bar plot of salt bridge formation between DPPC or DPPA molecules and lipase. Salt bridges were defined as sustained intermolecular interactions between a positively charged nitrogen group and a negatively charged oxygen group. Internal salt bridges (INT, gray) are competing intramolecular salt bridges occurring between lipase residues. (b) Intramolecular salt bridges forming between lipase residues.

rearrangement also contributes to the clustering of the lipases into islands to reduce the overall free energy of the system. Ultimately, since BCL forms less salt bridges with DPPA and more internal salt bridges (Figure 5b), the lipase islands desorb from the surface in discrete groups until the monolayer returns to its original, lipase-free state. There is also evidence of structural realignment after lipase insertion into DPPC monolayers that causes the broad hump in Figure 3, but the salt bridges between lipase and DPPC stabilize BCL in the monolayer.

Differences in Lipase Structure and Dynamics Based on Monolayer Surface Charge and Reciprocal Impacts on the Lipase-Embedded Surface. Molecular dynamics results show that lipase adopts substantial structural changes when introduced to charged surfactants to maximize favorable intermolecular interactions. Taken with the results given above, structural alignment techniques, clustering, and SASA analyses are used to interrogate the major structural and dynamic differences between lipase systems.

Table 1 shows the results of surface area analyses on BCL categorized by polar and nonpolar surface areas, as well as lipid-embedded and solvent-accessible surface areas. In DPPA, the solvent-accessible surface area increases from its starting structure by 19%, compared to 0% for BCL in DPPC. This can be attributed to the partial unraveling of the lipase in response to exposure to the negatively charged interface, coordinating its positive charges with negatively charged surfactants, and reducing negative-to-negative charge interactions. Insights into this structural change can be seen in Figure 6e. Compared to BCL in DPPC, BCL in DPPA achieves a final conformation with 11 nm^2 more solvent-exposed polar residues and 6 nm^2 more solvent-exposed nonpolar residues. While the total percentage of solvent-exposed surface area increases, the percentage of the lipid-embedded surface area stays the same, differing from the starting structure by at most 4% in the case of DPPC, with negligible differences in the total lipid-embedded surface area between the two final lipase

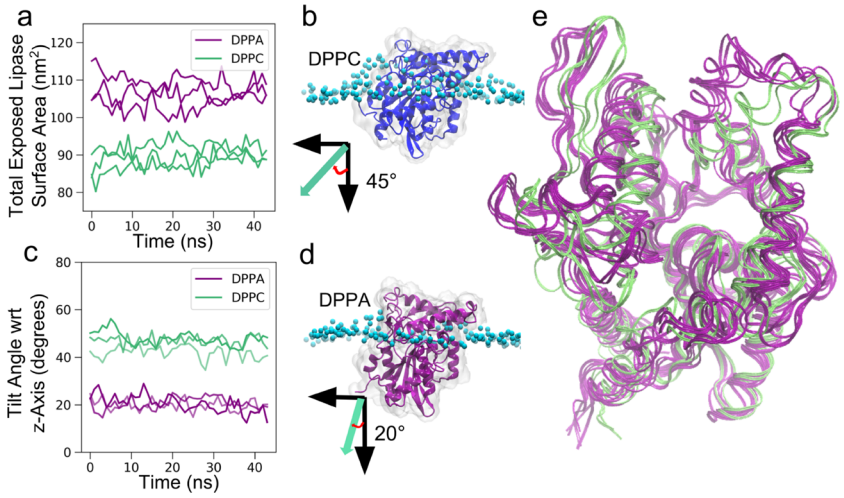

Figure 6. Structure of lipase and the lipase–monolayer complex changes based on surfactant charge, demonstrated by notable changes in lipase solvent-accessible surface area, angle of embedment into the monolayer, and structural clustering. (a) Total solvent-exposed lipase surface area by surfactant; (b) orientation of lipase (blue) in DPPC with the phosphate headgroups represented as cyan spheres; (c) tilt angle, defined by the vectors associated with internal β-sheets with respect to the z-axis; (d) orientation of lipase (purple) in DPPA with the phosphate headgroups represented as cyan spheres; (e) results of Gromos clustering analyses: two lipase structures from DPPC simulations (green) representing the top 50% of contributing clusters are overlaid with five lipase structures from DPPA simulations (purple) representing the top 35% of contributing clusters.

DOI: 10.1021/acs.langmuir.9b00689
Langmuir 2019, 35, 9050–9060

Table 1. Surface Area Analysis on Hydrophobic and Polar Residues Exposed to Solvent (Exposed) and Lipid (Embedded) for MD Simulations at Surface Areas of 47 Å^2/Lipid

lipase residues	initial structure[a] (nm^2)	DPPA (nm^2)	DPPC (nm^2)	Δ (nm^2) (DPPA−DPPC)
polar + charged exposed	54 ± 2	63 ± 3 (+16%)[b]	± 2 (−4%)	+11 ± 2
hydrophobic exposed	34 ± 2	±33 (+26%)	±3 (+8%)	+6 ± 2
total exposed	89 ± 4	106 ± 4 (+19%)	± 4 (+0%)	+17 ± 3
polar + charged embedded	19 ± 1	±32 (+0%)	± 2 (+10%)	−2 ± 2
hydrophobic embedded	38 ± 1	37 ± 2 (−3%)	±2 (−11%)	+3 ± 2
total embedded	57 ± 1	56 ± 2 (−2%)	±3 (−4%)	+1 ± 2

[a]Surface areas of initial postequilibration structures differed from each other by <1%. [b]Difference between the average and initial structures.

conformations. Surface areas for lipids interacting with lipase are given in Table S1. Figure 6a shows the total lipase surface area over the final 50 ns of each replicate.

Gromos clustering was used to highlight the major structural and dynamic differences between the two lipase-embedded monolayer systems (Figure 6e).[74] In total, BCL embedded in DPPC attained 33 clusters, while BCL in DPPA attained 164. The top 80% of contributing clusters are given in Table S2. For BCL in DPPC, approximately 60% of simulation time is dominated by two BCL conformations, shown in Figure 6e, with the dominant cluster contributing to 43% of frames. In contrast, in DPPA, the same percentage of simulation time is dominated by 11 different conformations, with the highest contributing conformation representing only 10% of frames. For simplicity, Figure 6e only shows five of these conformations, representing 34% of total simulation frames. It is clear that the major contributing clusters differ significantly from each other in each surfactant type. Clustering results indicate that BCL is highly flexible in DPPA and rigid in DPPC, which is supported by our salt bridge analysis. Due to the high number of salt bridges formed between BCL and DPPC, we would expect the enzyme to be more rigid than in DPPA, forming a stable DPPC−lipase complex. Conversely, the lack of salt bridges formed between BCL in DPPA allows the enzyme to be more dynamic, sampling approximately 5-fold more conformational states than in DPPC. Clustering results, taken together with a thorough analysis of electrostatic interactions, provide molecular support for the destabilization of lipase at anionic surfaces and stabilization at zwitterionic surfaces.

Finally, we investigated how electrostatics govern the overall structure of the protein-embedded monolayer (Figures 6 and S9). Figure 6b−d shows a comparison between orientations of the lipase at the surface. Figure 6c shows the evolution of the lipase tilt angle over the final 50 ns of each simulation, and Figure 6b,d shows MD snapshots of the lipase oriented in their respective lipids. In DPPC, BCL adopts a more tilted structure compared to BCL in DPPA, with the lipase tilting to a 45° angle with respect to the z-axis in DPPC versus only 20° in DPPA. In both cases, the hydrophobic active site helices are embedded in the lipids, but they achieve varying orientations in the monolayer plane. In DPPA, the loop formed by helices 4 and 5 lies in the plane of the headgroups, while in DPPC, the loop twists out of the plane (Figures 6b,d and S10). The surfactant headgroups in DPPC appear to scatter across the surface of lipase, increasing monolayer curvature, while the headgroups in DPPA remain more planar (Figure 2a).

These results indicate that monolayer surface charges govern large conformational changes in lipase to maximize favorable intermolecular interactions, which, in turn, impacts the structure of the surface. Since the total embedded surface area given in Table 1 does not change, it is likely that while van der Waals interactions may impact the partitioning of lipase to an aqueous−organic interface, they only play a small role in its overall stability in monolayers.[72,73] As suggested previously, this is to be expected, given that the hydrocarbon chain length limits the organic phase depth at the phospholipid interface. The unwinding of the lipase in DPPA can be attributed to significant repulsive electrostatic interactions between the negatively charged residues on BCL and the negatively charged phosphate headgroups. The few sites on BCL available for binding to DPPA—charged residues LYS 22, ARG297, and ARG258—coordinate with the phosphate headgroups in the monolayer plane. In DPPC, because there are cationic and anionic BCL residues available for binding, the lipase is stabilized in its open crystal structure conformation, and the phosphate headgroups disperse across the lipase surface, increasing local curvature and decreasing lipid-packing order. Since the surfactants in real SSA surfaces are likely to be variable in charge, as well as in lipid composition, we postulate that these results will extend to real SSA systems.

We suggest here that the stability of lipase-embedded monolayer surfaces is dictated by electrostatic interactions and that the interactions induce changes in the folded structure and dynamics of the enzyme, the packing of the lipids, and the overall structure and dynamics of the resulting protein-embedded surface. Because the structure of the enzyme changes with the surfactant charge, it is likely that the activity of lipase also changes, making it possible that, depending on details of the SSA surface composition, lipase could differentially act on and transform its surrounding lipid environment while in aerosol form. Furthermore, the dynamics of the surface are likely to modulate multiphase and heterogeneous atmospheric chemistry, where rigidity may enhance the ability of a surface to template into ice crystals, and flexibility could enhance gas or water transport across the surface.[75−78]

CONCLUSIONS

The results of this study suggest that electrostatic interactions between the external, charged amino acids on lipase and the individual charges on the surfactants play a significant role in the stability of lipases at the monolayer surface, as well as in the resulting structural properties of that surface. We present MD studies of BCL embedded in a lipid monolayer as an aqueous−organic interface, where organic phase depth is dependent on the length of the lipid tail, and stability at the interface is dependent on coordinated intermolecular interactions between the protein and surfactant. We demonstrate that, while the negative charge on DPPA is not enough to stabilize lipase at high concentrations or high surface pressures, the presence of a zwitterionic headgroup as in DPPC causes a significant increase in the monolayer-lipase lifetime. Although real SSA

DOI: 10.1021/acs.langmuir.9b00689
Langmuir 2019, 35, 9050−9060

surfaces are unlikely to be homogeneous matrices of either DPPC or DPPA, they are likely to vary in surface charge distribution based on their lipid profiles. In the context of sea spray aerosol chemistry, where the aerosol surface modulates atmospheric multiphase and heterogeneous reactions, understanding the surfactant-dependent dynamics and fluctuation of protein to and from the surface could bring us closer to accurately depicting SSA properties in atmospheric chemistry and climate models.

■ ASSOCIATED CONTENT

Supporting Information

The Supporting Information is available free of charge on the ACS Publications website at DOI: 10.1021/acs.langmuir.9b00689.

Simulation system setup; simulation convergence analyses, including dihedral energy, total energy, SASA, and RMSD; production run script; the isotherms of DPPC and DPPA; the surface pressure increase after lipase injected underneath DPPC monolayer with a certain area and a certain starting surface pressure; the IRRAS spectrum of C−H stretching region for DPPC monolayer holding at 15 and 25 mN/m before and 5 min after lipase injection; the structure of DPPC and DPPA; density profiles of DPPC and DPPA phosphates coordinated with sodium ions; percent area change of pure DPPA and DPPC monolayers; lipase labeled; SASA analysis on total surface areas of hydrophobic and polar residues exposed to solvent and lipid; and results of Gromos clustering analysis (PDF)

■ AUTHOR INFORMATION

Corresponding Authors

*vhgrassian@ucsd.edu

*ramaro@ucsd.edu

ORCID

Rommie E. Amaro: 0000-0002-9275-9553

Vicki H. Grassian: 0000-0001-5052-0045

Author Contributions

‖M.L. and A.C.D. contributed equally to this work.

Notes

The authors declare no competing financial interest.

■ ACKNOWLEDGMENTS

This work was supported by the National Science Foundation through the Center for Aerosol Impacts on Chemistry of the Environment (CAICE), an NSF funded center for Chemical Innovation (CHE-1801971). Computing support was provided by NSF CHE060073N to REA. The authors want to thank Dr Mona Shrestha and Dr Liubin Huang for helpful discussions on the experimental designs. The authors would also like to thank Nicholas Wauer for insightful suggestions in the MD analyses.

■ REFERENCES

(1) Reifenrath, R. Chemical Analysis of the Lung Alveolar Surfactant Obtained by Alveolar Micropuncture. *Respir. Physiol.* **1973**, *19*, 35−46.

(2) Butovich, I. A. Tear Film Lipids. *Exp. Eye Res.* **2013**, *117*, 4−27.

(3) Forestieri, S. D.; Staudt, S. M.; Kuborn, T. M.; Faber, K.; Ruehl, C. R.; Bertram, T. H.; Cappa, C. D. Establishing the Impact of Model Surfactants on Cloud Condensation Nuclei Activity of Sea Spray Aerosols. *Atmos. Chem. Phys.* **2018**, *18*, 10985−11005.

(4) DeMott, P. J.; Mason, R. H.; McCluskey, C. S.; Hill, T. C. J.; Perkins, R. J.; Desyaterik, Y.; Bertram, A. K.; Trueblood, J. V.; Grassian, V. H.; Qiu, Y.; et al. Ice Nucleation by Particles Containing Long-Chain Fatty Acids of Relevance to Freezing by Sea Spray Aerosols. *Environ. Sci. Process. Impacts* **2018**, *20*, 1559−1569.

(5) Collins, D. B.; Ault, A. P.; Moffet, R. C.; Ruppel, M. J.; Cuadra-Rodriguez, L. A.; Guasco, T. L.; Corrigan, C. E.; Pedler, B. E.; Azam, F.; Aluwihare, L. I.; et al. Impact of Marine Biogeochemistry on the Chemical Mixing State and Cloud Forming Ability of Nascent Sea Spray Aerosol. *J. Geophys. Res.: Atmos.* **2013**, *118*, 8553−8565.

(6) Fuentes, E.; Coe, H.; Green, D.; McFiggans, G. On the Impacts of Phytoplankton-Derived Organic Matter on the Properties of the Primary Marine Aerosol − Part 2: Composition, Hygroscopicity and Cloud Condensation Activity. *Atmos. Chem. Phys.* **2011**, *11*, 2585−2602.

(7) Cosman, L. M.; Bertram, A. K. Reactive Uptake of N_2O_5 on Aqueous H_2SO_4 Solutions Coated with 1-Component and 2-Component Monolayers. *J. Phys. Chem. A* **2008**, *112*, 4625−4635.

(8) Ryder, O. S.; Campbell, N. R.; Shaloski, M.; Al-Mashat, H.; Nathanson, G. M.; Bertram, T. H. Role of Organics in Regulating ClNO 2 Production at the Air−Sea Interface. *J. Phys. Chem. A* **2015**, *119*, 8519−8526.

(9) Gord, J. R.; Zhao, X.; Liu, E.; Bertram, T. H.; Nathanson, G. M. Control of Interfacial Cl_2 and N_2O_5 Reactivity by a Zwitterionic Phospholipid in Comparison with Ionic and Uncharged Surfactants. *J. Phys. Chem. A* **2018**, *122*, 6593−6604.

(10) Tervahattu, H.; Hartonen, K.; Kerminen, V.-M.; Kupiainen, K.; Aarnio, P.; Koskentalo, T.; Tuck, A.; Vaida, V. New Evidence of an Organic Layer on Marine Aerosols. *J. Geophys. Res.* **2002**, *107*, 4053.

(11) Mccluskey, C. S.; Hill, T. C. J.; Sultana, C. M.; Laskina, O.; Trueblood, J.; Santander, M. V.; Beall, C. M.; Michaud, J. M.; Kreidenweis, S. M.; Prather, K. A.; et al. A Mesocosm Double Feature: Insights into the Chemical Makeup of Marine Ice Nucleating Particles. *J. Atmos. Sci.* **2018**, *75*, 2405−2423.

(12) Shrestha, M.; Luo, M.; Li, Y.; Xiang, B.; Xiong, W.; Grassian, V. H. Let There Be Light: Stability of Palmitic Acid Monolayers at the Air/Salt Water Interface in the Presence and Absence of Simulated Solar Light and a Photosensitizer. *Chem. Sci.* **2018**, *9*, 5716−5723.

(13) Tang, C. Y.; Huang, Z.; Allen, H. C. Binding of Mg 2+and Ca 2+to Palmitic Acid and Deprotonation of the COOH Headgroup Studied by Vibrational Sum Frequency Generation Spectroscopy. *J. Phys. Chem. B* **2010**, *114*, 17068−17076.

(14) Adams, E. M.; Casper, C. B.; Allen, H. C. Effect of Cation Enrichment on Dipalmitoylphosphatidylcholine (DPPC) Monolayers at the Air-Water Interface. *J. Colloid Interface Sci.* **2016**, *478*, 353−364.

(15) Zhang, T.; Fiamingo, M.; Allen, H. C. Trace Metal Enrichment Driven by Phosphate Functional Group Binding Selectivity. *J. Geophys. Res.: Oceans* **2018**, *123*, 5286−5297.

(16) Cochran, R. E.; Laskina, O.; Jayarathne, T.; Laskin, A.; Laskin, J.; Lin, P.; Sultana, C.; Lee, C.; Moore, K. A.; Cappa, C. D.; et al. Analysis of Organic Anionic Surfactants in Fine and Coarse Fractions of Freshly Emitted Sea Spray Aerosol. *Environ. Sci. Technol.* **2016**, *50*, 2477−2486.

(17) Michaud, J. M.; Thompson, L. R.; Kaul, D.; Espinoza, J. L.; Richter, R. A.; Xu, Z. Z.; Lee, C.; Pham, K. M.; Beall, C. M.; Malfatti, F.; et al. Taxon-Specific Aerosolization of Bacteria and Viruses in an Experimental Ocean-Atmosphere Mesocosm. *Nat. Commun.* **2018**, *9*, No. 2017.

(18) Lee, H. D.; Estillore, A. D.; Morris, H. S.; Ray, K. K.; Alejandro, A.; Grassian, V. H.; Tivanski, A. V. Direct Surface Tension Measurements of Individual Sub-Micrometer Particles Using Atomic Force Microscopy. *J. Phys. Chem. A* **2017**, *121*, 8296−8305.

(19) Wang, X.; Sultana, C. M.; Trueblood, J.; Hill, T. C. J.; Malfatti, F.; Lee, C.; Laskina, O.; Moore, K. A.; Beall, C. M.; McCluskey, C. S.; et al. Microbial Control of Sea Spray Aerosol Composition: A Tale of Two Blooms. *ACS Cent. Sci.* **2015**, *1*, 124−131.

DOI: 10.1021/acs.langmuir.9b00689
Langmuir 2019, 35, 9050−9060

(20) Cochran, R. E.; Laskina, O.; Trueblood, J.; Estillore, A. D.; Morris, H. S.; Jayarathne, T.; Sultana, C. M.; Lee, C.; Lin, P.; Laskin, J.; et al. Molecular Characterization of Sea Spray Particles: Influence of Ocean Biology on Particle Composition and Interaction with Water. *Chem* **2017**, *2*, 655−667.
(21) Keene, W. C.; Maring, H.; Maben, J. R.; Kieber, D. J.; Pszenny, A. A. P.; Dahl, E. E.; Izaguirre, M. A.; Davis, A. J.; Long, M. S.; Zhou, X.; et al. Chemical and Physical Characteristics of Nascent Aerosols Produced by Bursting Bubbles at a Model Air-Sea Interface. *J. Geophys. Res.: Atmos.* **2007**, No. D10306.
(22) Ault, A. P.; Moffet, R. C.; Baltrusaitis, J.; Collins, D. B.; Ruppel, M. J.; Cuadra-Rodriguez, L. A.; Zhao, D.; Guasco, T. L.; Ebben, C. J.; Geiger, F. M.; et al. Size-Dependent Changes in Sea Spray Aerosol Composition and Properties with Different Seawater Conditions. *Environ. Sci. Technol.* **2013**, *47*, 5603−5612.
(23) Jayarathne, T.; Sultana, C. M.; Lee, C.; Malfatti, F.; Cox, J. L.; Pendergraft, M. A.; Moore, K. A.; Azam, F.; Tivanski, A. V.; Cappa, C. D.; et al. Enrichment of Saccharides and Divalent Cations in Sea Spray Aerosol during Two Phytoplankton Blooms. *Environ. Sci. Technol.* **2016**, No. 2988.
(24) Duncan, S. L.; Larson, R. G. Comparing Experimental and Simulated Pressure-Area Isotherms for DPPC. *Biophys. J.* **2008**, No. 114215.
(25) Baoukina, S.; Mendez-Villuendas, E.; Tieleman, D. P. Molecular View of Phase Coexistence in Lipid Monolayers. *J. Am. Chem. Soc.* **2012**, *134*, 17543−17553.
(26) Habartová, A.; Roeselová, M.; Cwiklik, L. Investigation of Mixed Surfactant Films at Water Surface Using Molecular Dynamics Simulations. *Langmuir* **2015**, *31*, 11508−11515.
(27) Lin, W.; Clark, A. J.; Paesani, F. Effects of Surface Pressure on the Properties of Langmuir Monolayers and Interfacial Water at the Air-Water Interface. *Langmuir* **2015**, *31*, 2147−2156.
(28) Schiffer, J. M.; Mael, L. E.; Prather, K. A.; Amaro, R. E.; Grassian, V. H. Sea Spray Aerosol: Where Marine Biology Meets Atmospheric Chemistry. *ACS Cent Sci.* **2019**, *19*, No. 46.
(29) Chapus, C.; Rovery, M.; Sarda, L.; Verger, R. Minireview on Pancreatic Lipase and Colipase. *Biochimie* **1988**, *70*, 1223−1233.
(30) Sánchez, D. A.; Tonetto, G. M.; Ferreira, M. L. *Burkholderia Cepacia* Lipase: A Versatile Catalyst in Synthesis Reactions. *Biotechnol. Bioeng.* **2018**, *115*, 6−24.
(31) Svendsen, A. Lipase Protein Engineering. *Biochim. Biophys. Acta, Protein Struct. Mol. Enzymol.* **2000**, *1543*, 223−238.
(32) Vial, L.; Chapalain, A.; Groleau, M.-C.; Déziel, E. The Various Lifestyles of the *Burkholderia Cepacia* Complex Species: A Tribute to Adaptation. *Environ. Microbiol.* **2011**, *13*, 1−12.
(33) Maravić, A.; Skočibušić, M.; Šprung, M.; Šamanić, I.; Puizina, J.; Pavela-Vrančić, M. Occurrence and Antibiotic Susceptibility Profiles of *Burkholderia Cepacia* Complex in Coastal Marine Environment. *Int. J. Environ. Health Res.* **2012**, *22*, 531−542.
(34) Malfatti, F.; Lee, C.; Tinta, T.; Pendergraft, M. A.; Celussi, M.; Zhou, Y.; Sultana, C. M.; Rotter, A.; Axson, J. L.; Collins, D. B.; et al. Detection of Active Microbial Enzymes in Nascent Sea Spray Aerosol: Implications for Atmospheric Chemistry and Climate. *Environ. Sci. Technol. Lett.* **2019**, No. 699.
(35) Aller, J. Y.; Kuznetsova, M. R.; Jahns, C. J.; Kemp, P. F. The Sea Surface Microlayer as a Source of Viral and Bacterial Enrichment in Marine Aerosols. *J. Aerosol Sci.* **2005**, *36*, 801−812.
(36) Schiffer, J. M.; Luo, M.; Dommer, A. C.; Thoron, G.; Pendergraft, M.; Santander, M. V.; Lucero, D.; Pecora De Barros, E.; Prather, K. A.; Grassian, V. H.; et al. Impacts of Lipase Enzyme on the Surface Properties of Marine Aerosols. *J. Phys. Chem. Lett* **2018**, *9*, 22.
(37) Pires De Oliveira, I.; Jara, G. E.; Martí Nez, L. Molecular Mechanism of Activation of *Burkholderia Cepacia* Lipase at Aqueous-Organic Interfaces. *Phys. Chem. Chem. Phys* **2017**, *19*, 31499.
(38) Barbe, S.; Lafaquière, V.; Guieysse, D.; Monsan, P.; Remaud-Siméon, M.; André, I. Insights into Lid Movements of *Burkholderia Cepacia* Lipase Inferred from Molecular Dynamics Simulations. *Proteins* **2009**, *77*, 509−523.
(39) Vial, L.; Chapalain, A.; Groleau, M.-C.; Déziel, E. The Various Lifestyles of the *Burkholderia Cepacia* Complex Species: A Tribute to Adaptation. *Environ. Microbiol.* **2011**, *13*, 1−12.
(40) Sánchez, D. A.; Tonetto, G. M.; Ferreira, M. L. *Burkholderia Cepacia* Lipase: A Versatile Catalyst in Synthesis Reactions. *Biotechnol. Bioeng.* **2018**, *115*, 6−24.
(41) Sasso, F.; Natalello, A.; Castoldi, S.; Lotti, M.; Santambrogio, C.; Grandori, R. *Burkholderia Cepacia* Lipase Is a Promising Biocatalyst for Biofuel Production. *Biotechnol. J.* **2016**, *11*, 954−960.
(42) Eftaiha, A. F.; Wanasundara, S. N.; Paige, M. F.; Bowles, R. K. Exploring the Impact of Tail Polarity on the Phase Behavior of Single Component and Mixed Lipid Monolayers Using a MARTINI Coarse-Grained Force Field. *J. Phys. Chem. B* **2016**, *120*, 7641−7651.
(43) Szőri, M.; Jedlovszky, P.; Roeselová, M. Water Adsorption on Hydrophilic and Hydrophobic Self-Assembled Monolayers as Proxies for Atmospheric Surfaces. A Grand Canonical Monte Carlo Simulation Study. *Phys. Chem. Chem. Phys.* **2010**, *12*, 4604.
(44) Adams, E. M.; Wellen, B. A.; Thiraux, R.; Reddy, S. K.; Vidalis, A. S.; Paesani, F.; Allen, H. C. Sodium − Carboxylate Contact Ion Pair Formation Induces Stabilization of Palmitic Acid Monolayers at High PH. *Phys. Chem. Chem. Phys.* **2017**, *19*, 10481−10490.
(45) Zhang, T.; Brantley, S. L.; Verreault, D.; Dhankani, R.; Corcelli, S. A.; Allen, H. C. Effect of PH and Salt on Surface PK a of Phosphatidic Acid Monolayers. *Langmuir* **2018**, *34*, 530−539.
(46) Sandhiya, L.; Kolandaivel, P.; Senthilkumar, K. Oxidation and Nitration of Tyrosine by Ozone and Nitrogen Dioxide: Reaction Mechanisms and Biological and Atmospheric Implications. *J. Phys. Chem. B* **2014**, *118*, 3479−3490.
(47) Liu, F.; Lakey, P. S. J.; Berkemeier, T.; Tong, H.; Kunert, A. T.; Meusel, H.; Cheng, Y.; Su, H.; Fröhlich-Nowoisky, J.; Lai, S.; et al. Atmospheric Protein Chemistry Influenced by Anthropogenic Air Pollutants: Nitration and Oligomerization upon Exposure to Ozone and Nitrogen Dioxide. *Faraday Discuss.* **2017**, *200*, 413−427.
(48) Estillore, A. D.; Trueblood, J. V.; Grassian, V. H. Atmospheric Chemistry of Bioaerosols: Heterogeneous and Multiphase Reactions with Atmospheric Oxidants and Other Trace Gases. *Chem. Sci.* **2016**, *7*, 6604−6616.
(49) Marsh, D. Protein Modulation of Lipids, and Vice-Versa, in Membranes. *Biochim. Biophys. Acta, Biomembr.* **2008**, *1778*, 1545−1575.
(50) Mouchlis, V. D.; Chen, Y.; McCammon, J. A.; Dennis, E. A. Membrane Allostery and Unique Hydrophobic Sites Promote Enzyme Substrate Specificity. *J. Am. Chem. Soc.* **2018**, *140*, 3285−3291.
(51) Mouchlis, V. D.; Bucher, D.; McCammon, J. A.; Dennis, E. A. Membranes Serve as Allosteric Activators of Phospholipase A2, Enabling It to Extract, Bind, and Hydrolyze Phospholipid Substrates. *Proc. Natl. Acad. Sci. U.S.A.* **2015**, *112*, E516−E525.
(52) Adams, E.; Allen, H.; Adams, E. M.; Allen, H. C. Palmitic Acid on Salt Subphases and in Mixed Monolayers of Cerebrosides: Application to Atmospheric Aerosol Chemistry. *Atmosphere* **2013**, *4*, 315−336.
(53) Fridlind, A. M.; Jacobson, M. Z. A Study of Gas-Aerosol Equilibrium and Aerosol PH in the Remote Marine Boundary Layer during the First Aerosol Characterization Experiment (ACE 1). *J. Geophys. Res.: Atmos.* **2000**, *105*, 17325−17340.
(54) Dluhy, R. A. Quantitative external reflection infrared spectroscopic analysis of insoluble monolayers spread at the air-water interface. *J. Phys. Chem.* **1986**, *90*, No. 33.
(55) Sierra-Hern Andez, M. R.; Allen, H. C. Incorporation and Exclusion of Long Chain Alkyl Halides in Fatty Acid Monolayers at the Air-Water Interface. *Langmuir* **2010**, *26*, 18806−18816.
(56) Jo, S.; Kim, T.; Iyer, V. G.; Im, W. CHARMM-GUI: A Web-Based Graphical User Interface for CHARMM. *J. Comput. Chem.* **2008**, *29*, 2967−2970.
(57) Huang, J.; Mackerell, A. D. CHARMM36 All-Atom Additive Protein Force Field: Validation Based on Comparison to NMR Data. *J. Comput. Chem.* **2013**, *34*, 2135−2145.

DOI: 10.1021/acs.langmuir.9b00689
Langmuir 2019, 35, 9050−9060

(58) Marrink, S. J.; Tieleman, D. P. *Structure and Dynamics of Lipid Monolayers: Theory and Applications*; Biomembrane Frontiers: Humana Press, 2009; pp 75−76.
(59) Madhavi Sastry, G.; Adzhigirey, M.; Day, T.; Annabhimoju, R.; Sherman, W. Protein and Ligand Preparation: Parameters, Protocols, and Influence on Virtual Screening Enrichments. *J. Comput.-Aided Mol. Des.* **2013**, *27*, 221−234.
(60) Schrag, J. D.; Li, Y.; Cygler, M.; Lang, D.; Burgdorf, T.; Hecht, H. J.; Schmid, R.; Schomburg, D.; Rydel, T. J.; Oliver, J. D.; et al. The Open Conformation of a Pseudomonas Lipase. *Structure* **1997**, *5*, 187−202.
(61) Lomize, M. A.; Pogozheva, I. D.; Joo, H.; Mosberg, H. I.; Lomize, A. L. OPM Database and PPM Web Server: Resources for Positioning of Proteins in Membranes. *Nucleic Acids Res.* **2012**, *40*, D370−D376.
(62) Berendsen, H. J. C.; van der Spoel, D.; van Drunen, R. GROMACS: A Message-Passing Parallel Molecular Dynamics Implementation. *Comput. Phys. Commun.* **1995**, *91*, 43−56.
(63) Abraham, M. J.; Murtola, T.; Schulz, R.; Páll, S.; Smith, J. C.; Hess, B.; Lindahl, E. GROMACS: High Performance Molecular Simulations through Multi-Level Parallelism from Laptops to Supercomputers. *SoftwareX* **2015**, *1−2*, 19−25.
(64) Towns, J.; Cockerill, T.; Dahan, M.; Foster, I.; Gaither, K.; Grimshaw, A.; Hazlewood, V.; Lathrop, S.; Lifka, D.; Peterson, G. D.; et al. XSEDE: Accelerating Scientific Discovery. *Comput. Sci. Eng.* **2014**, *16*, 62−74.
(65) Nystrom, N. A.; Levine, M. J.; Roskies, R. Z.; Scott, J. R. In *Bridges: A Uniquely Flexible HPC Resource for New Communities and Data Analytics*, Proceedings of the 2015 XSEDE Conference on Scientific Advancements Enabled by Enhanced Cyberinfrastructure - XSEDE '15, 2015; pp 1−8.
(66) Pérez, F.; Granger, B. E. IPython: A System for Interactive Scientific Computing Python: An Open and General- Purpose Environment. *Comput. Sci. Eng.* **2007**, *9*, 21−29.
(67) Phillips, M. C.; Chapman, D. Monolayer Characteristics of Saturated 1,2-Diacyl Phosphatidylcholines (Lecithins) and Phosphatidylethanolamines at the Air-Water Interface. *Biochim. Biophys. Acta, Biomembr.* **1968**, *163*, 301−313.
(68) Adams, E. M.; Verreault, D.; Jayarathne, T.; Cochran, R. E.; Stone, E. A.; Allen, H. C. Surface Organization of a DPPC Monolayer on Concentrated SrCl2 and ZnCl2 Solutions. *Phys. Chem. Chem. Phys.* **2016**, *18*, 32345−32357.
(69) Hunt, R. D.; Mitchell, M. L.; Dluhy, R. A. The Interfacial Structure of Phospholipid Monolayer Films: An Infrared Reflectance Study. *J. Mol. Struct.* **1989**, *214*, 93−109.
(70) Orendorff, C. J.; Ducey, M. W.; Pemberton, J. E. Quantitative Correlation of Raman Spectral Indicators in Determining Conformational Order in Alkyl Chains. *J. Phys. Chem. A* **2002**, 6991−6998.
(71) Snyder, R. G.; Hsu, S. L.; Krimm, S. Vibrational Spectra in the C-H Stretching Region and the Structure of the Polymetheylene Chain. *Spectrochim. Acta, Part A* **1978**, *34*, 395−406.
(72) Wallach, D. F. H.; Verma, S. P.; Fookson, J. Application of Laser Raman and Infrared Spectroscopy to the Analysis of Membrane Structure. *Biochim. Biophys. Acta* **1979**, *559*, 153−208.
(73) Karvaly, B.; Loshchilova, E. Comments on the Quantitative Interpretation of Biomembrane Structure by Raman Spectroscopy. *Biochim. Biophys. Acta, Biomembr.* **1977**, *470*, 492−496.
(74) Huang, W.-N.; Sue, S.-C.; Wang, D.-S.; Wu, P.-L.; Wu, W. Peripheral Binding Mode and Penetration Depth of Cobra Cardiotoxin on Phospholipid Membranes as Studied by a Combined FTIR and Computer Simulation Approach. *Biochemistry* **2003**, *42*, 7457−7466.
(75) Meister, A.; Nicolini, C.; Waldmann, H.; Kuhlmann, J.; Kerth, A.; Winter, R.; Blume, A. Insertion of Lipidated Ras Proteins into Lipid Monolayers Studied by Infrared Reflection Absorption Spectroscopy (IRRAS). *Biophys. J.* **2006**, *91*, 1388−1401.
(76) Mendelsohn, R.; Brauner, J. W.; Gericke, A. External Infrared Reflection Absorption Spectrometry of Monolayer Films at the Air-Water Interface. *Annu. Rev. Phys. Chern* **1995**, *46*, 305−339.
(77) Mendelsohn, R.; Mao, G.; Flach, C. R. Infrared Reflection-Absorption Spectroscopy: Principles and Applications to Lipid-Protein Interaction in Langmuir Films. *Biochim. Biophys. Acta* **2010**, *1798*, 788−800.
(78) Rusdi, M.; Moroi, Y. Study on Water Evaporation through 1-Alkanol Monolayers by the Thermogravimetry Method. *J. Colloid Interface Sci.* **2004**, *272*, 472−479.
(79) La Mer, V. K.; Healy, T. W.; Aylmore, L. A. G. The Transport of Water through Monolayers of Long-Chain n-Paraffinic Alcohols. *J. Colloid Sci.* **1964**, *19*, 673−684.
(80) McNamee, C. E.; Barnes, G. T.; Gentle, I. R.; Peng, J. B.; Steitz, R.; Probert, R. The Evaporation Resistance of Mixed Monolayers of Octadecanol and Cholesterol. *J. Colloid Interface Sci.* **1998**, *207*, 258−263.
(81) Barnes, G.; Bacon, K.; Ash, J. The Evaporation Resistances of Octadecanol-Cholesterol Mixed Monolayers. *J. Colloid Interface Sci.* **1980**, *76*, 263−264.
(82) Costin, I. S.; Barnes, G. T. The Purification of Long-Chain Alcohols for Monolayer Studies. *J. Colloid Interface Sci.* **1967**, *25*, 584−585.
(83) Brzozowska, A. M.; Duits, M. H. G.; Mugele, F. Stability of Stearic Acid Monolayers on Artificial Sea Water. *Colloids Surf., A* **2012**, *407*, 38−48.
(84) Patil, G. S.; Matthews, R. H.; Cornwell, D. G. Kinetics of the Processes of Desorption from Fatty Acid Monolayers. *J. Lipid Res.* **1973**, *14*, 26−31.
(85) Basu, S.; Biswas, P. Salt-Bridge Dynamics in Intrinsically Disordered Proteins: A Trade-off between Electrostatic Interactions and Structural Flexibility. *Biochim. Biophys. Acta, Proteins Proteomics* **2018**, *1866*, 624−641.
(86) Basu, S.; Mukharjee, D. Salt-Bridge Networks within Globular and Disordered Proteins: Characterizing Trends for Designable Interactions. *J. Mol. Model.* **2017**, *23*, 206.
(87) Gruia, A. D.; Fischer, S.; Smith, J. C. Molecular Dynamics Simulation Reveals a Surface Salt Bridge Forming a Kinetic Trap in Unfolding of Truncated Staphylococcal Nuclease. *Proteins* **2003**, *50*, 507−515.
(88) Aliste, M. P.; MacCallum, J. L.; Tieleman, D. P. Molecular Dynamics Simulations of Pentapeptides at Interfaces: Salt Bridge and Cation−π Interactions. *Biochemistry* **2003**, *42*, 8976−8987.

DOI: 10.1021/acs.langmuir.9b00689
Langmuir 2019, 35, 9050−9060